The Role of Ply Buckling in the Compressive Failure of Graphite/Epoxy Tubes

Anthony J. Vizzini* and Paul A. Lagace†
Massachusetts Institute of Technology, Cambridge, Massachusetts

A study was conducted to look at the interaction of in-plane and out-of-plane compressive failure modes of graphite/epoxy. In the study, 75 six-ply graphite/epoxy tubes were manufactured and tested in uniaxial compression. Failure stresses and modes were determined and compared with those predicted from an in-plane fracture criterion and an equilibrium shell buckling analysis. There were large discrepancies between the experimental results and these theoretical predictions. These predictions did not account for a failure mode exhibited by several laminates: individual plies buckling and delaminating away from the remaining plies. A "ply buckling" model is introduced to explain these discrepancies. There is good correlation between the experimental failure modes and stresses with the "feasible" failure region defined by this ply buckling model.

Nomenclature

A_{mn}, B_{mn}, C_{mn}	= coefficients in buckling displacement mode
CV	= coefficient of variation
E_L	= longitudinal modulus
E_T	= transverse modulus
$F_{\alpha\beta}, F_{\alpha\beta\sigma\gamma}$	= strength coefficients in stress interaction criterion
G_{LT}	= shear modulus
L	= length
L/R	= length-to-radius ratio
m	= number of half-sine waves in the longitudinal direction in buckling displacement modes
n	= number of half-sine waves in the circumferential direction in buckling displacement modes
R	= radius
u°	= longitudinal displacement of midplane in shell equilibrium method
v°	= circumferential displacement of midplane in shell equilibrium method
w	= radial displacement in shell equilibrium method
x	= coordinate in longitudinal direction
$\sigma_{\alpha\beta}$	= stress ($\alpha, \beta = 1, 2$)
θ	= lamination angle
Φ	= coordinate in circumferential direction
ν_{LT}	= major Poisson's ratio

Introduction

THE compressive failure of graphite/epoxy structures is often the result of local instabilities. Instabilities have been observed on the macroscopic scale (plate buckling and crippling) and on the microscopic scale (fiber buckling). Much theoretical and experimental work has been done in trying to isolate and describe the various failure mechanisms. Greszczuk,[1] de Ferrian and Harris,[2] and Lager and June[3] have observed fiber buckling failure modes and have correlated the results with theoretical predictions with some success. However, the failure modes of graphite/epoxy structures observed under compression are generally macroscopic instabilities involving buckling of the entire laminate or parts thereof. At this level, the composite laminate can be viewed as an orthotropic plate with "smeared" elastic properties. Solutions such as those by Timoshenko[4] for a specially orthotropic plate and Whitney[5] for generally anisotropic cylindrical plates can be used. Various edge constraints have been explored by authors.

In this study, 75 six-ply graphite/epoxy tubes were tested in uniaxial compression in order to observe the failure modes. The original intent of the work was the development of a compressive ultimate specimen to determine compressive fracture stresses for various laminates. In the past, a number of specimens have been developed to obtain compressive ultimates such as the sandwich beam used in four-point bending.[6] A number of these specimens require supporting jigs such as the IITRI fixture[7] and that recommended by ASTM Standard D 3410-75.[8] Many of these specimens impose artifical boundary conditions on the specimen. For example, supporting jigs, while preventing overall buckling (as is their purpose), also prevent the legitimate local failure of ply buckling. This phenomenon is discussed within.

In this investigation, it was hoped that a mixture of modes (in-plane fracture and out-of-plane buckling) would occur, allowing for a study of the relationship and the interaction between fracture and local instabilities. However, a third mode of failure was revealed. This mode of failure resulted in the outer and inner radii plies partially or totally delaminating from the remaining plies, either at or prior to ultimate failure. Large discrepancies were observed between failure stresses predicted as based on in-plane fracture or shell buckling criteria and experimental failure stresses and failure modes. In this study, a model is proposed that aids in the understanding of the interacting mechanisms that can cause the apparently premature compressive failure of a laminated structure.

Failure Predictions

Two failure criteria were primarily employed in this study. The first is an in-plane fracture prediction based on the stress interaction criterion as proposed by Tsai and Wu.[9] The second is a shell buckling prediction based on the equilibrium method

Received March 13, 1984; presented as Paper 84-0963 at the AIAA/ASME/ASCE/AHS 25th Structures, Structural Dynamics and Materials Conference, Palm Springs, CA, May 14-16, 1984; revision submitted Feb. 25, 1985.

*Research Assistant, Technology Laboratory for Advanced Composites, Department of Aeronautics and Astronautics. Student Member AIAA.

†Assistant Professor, Aeronautics and Astronautics, Technology Laboratory for Advanced Composites, Department of Aeronautics and Astronautics. Member AIAA.

as discussed by Whitney and Sun.[10] The coordinate system used in these analysis is shown in Fig. 1.

The stress interaction criterion is a curve fit of experimental data to a quadratic polynomial. The two-dimensional tensorial form of the equation gives fracture to occur in a unidirectional ply for the condition

$$F_{1111}\sigma_{11}^2 + 2F_{1122}\sigma_{11}\sigma_{22} + F_{2222}\sigma_{22}^2 + 4F_{1212}\sigma_{12}^2 + F_{11}\sigma_{11} + F_{22}\sigma_{22} = 1 \quad (1)$$

Five of the six strength parameters (F_{1111}, F_{2222}, F_{11}, F_{22}, F_{22}, F_{1212}) are obtained by testing a single ply of the material in longitudinal tension, longitudinal compression, transverse tension, transverse compression, and shear. The sixth constant, F_{1212}, is the interaction term. It has been suggested[11] that this be set by likening the Tsai-Wu criterion to the Mises-Hencky criterion for isotropic materials. This gives the equation

$$F_{1122} = -\tfrac{1}{2}(F_{1111}F_{2222})^{1/2} \quad (2)$$

for the interaction term. The criterion is applied on the ply stresses in ply axes on a ply-by-ply basis using classical laminated plate theory and the basic unidirectional ply properties of the material. The values for Hercules AS1/3501-6 are $E_L = 130$ GPa, $E_T = 10.5$ GPa, $\nu_{LT} = 0.28$, $G_{LT} = 6.0$ GPa, longitudinal tensile strength = 1661 MPa, longitudinal compressive strength = 1698 MPa, transverse tensile strength = 53.9 MPa, transverse compressive strength = 221 MPa, and shear strength = 105 MPa. In this case, the stress at which the first ply fails is considered to be the in-plane fracture stress.

The equilibrium method for shell buckling determines the buckling stress by finding the minimum load that is necessary to maintain a buckled cylinder in equilibrium. The shape of the buckled tube is determined from a number of assumed modes. Each assumed shape can be made up of any number of modes. The approximate method developed by Whitney and Sun assumes the displacements to be of the form

$$u^\circ = A_{mn}\sin(m\pi x/L \pm n\Phi)$$
$$v^\circ = B_{mn}\sin(m\pi x/L \pm n\Phi)$$
$$w = C_{mn}\cos(m\pi x/L \pm n\Phi) \quad (3)$$

where m is the number of half-sine waves in the longitudinal direction and n the number of full sine waves in the circumferential direction. The load necessary for equilibrium of the cylinder can be found for each combination of n and m. Of these, the lowest load corresponds to the buckling stress and the n and m correspond to the initial buckling shape.

The equilibrium method is only an approximate solution for the buckling stress. Initial imperfections in the specimen will cause buckling prior to this predicted stress level. The equilibrium method thus represents an upper bound on the buckling load.

Experimental Program

A total of 73 six-ply graphite/epoxy tubes were initially manufactured and tested. Of the 73 tubes, 22 were $[0_6]$ laminates with length-to-radius ratios of 2-12. Two tubes had a $[90_6]$ layup with a nominal length-to-radius ratio of 5. The remaining 49 tubes had a nominal length-to-radius ratio of five and had layups of either $[\pm\theta/0]_s$ or $[0/\pm\theta]_s$. The values of the lamination angle θ are 10°, 20°, 30°, 35°, 40°, 45°, 60°, and 90°. The length-to-radius ratios were chosen so as to prevent Euler column buckling of the entire specimen. The entire test program is shown in Table 1. The nominal radius of all the specimens is 19.05 mm.

The material used throughout the program was AS1/3501-6 manufactured by Hercules. The material is supplied as a preimpregnated 305-mm-wide tape and is cut into plies and layed up into a rubber mandril. The tubes were cured on the same rubber mandril with the necessary cure materials as shown in Fig. 2. The cure took place in an autoclave and followed the manufacturer's recommended cycle of 1 h at 116°C and 2 h at 177°C with 0.59 MPa and a full vacuum (762 mm Hg) applied throughout. All specimens were postcured at 177°C in an oven for 8 h. The specimens were machined to the desired lengths on a milling machine adapted for graphite/epoxy with a water-cooled diamond-grit blade.

The thickness, inside and outside diameters, and length were measured at several locations of each tube. The average thickness of all the specimens is 0.78 mm with a coefficient of variation of 3.2%. The average diameter of the midsurface of the specimens is 39.9 mm with a coefficient of variation of 0.61%. For calculation purposes, nominal values of 0.804 mm for the thickness and 38.1 mm for the diameter were used (the manufacturer's nominal per ply thickness is 0.134 mm). This

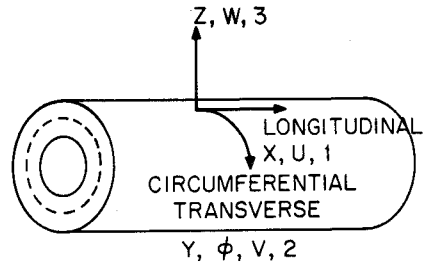

Fig. 1 Tube coordinate system.

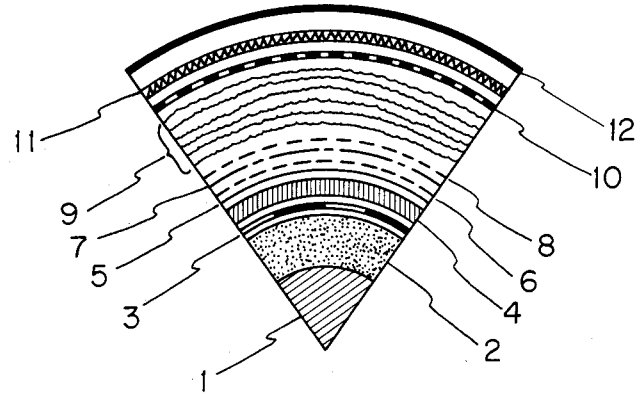

Fig. 2 Cross section of cure materials.

Table 1 Experimental test program

	Laminates		
θ°	$[\theta_6]$	$[\pm\theta/0]_s$	$[0/\pm\theta]_s$
0	22[a]	—	—
10	—	4	4
20	—	4	4
30	—	4	4
35	—	2	2
40	—	2	2
45	—	5	4
60	—	2	2
90	2	2	2

[a]Number of specimens tested.

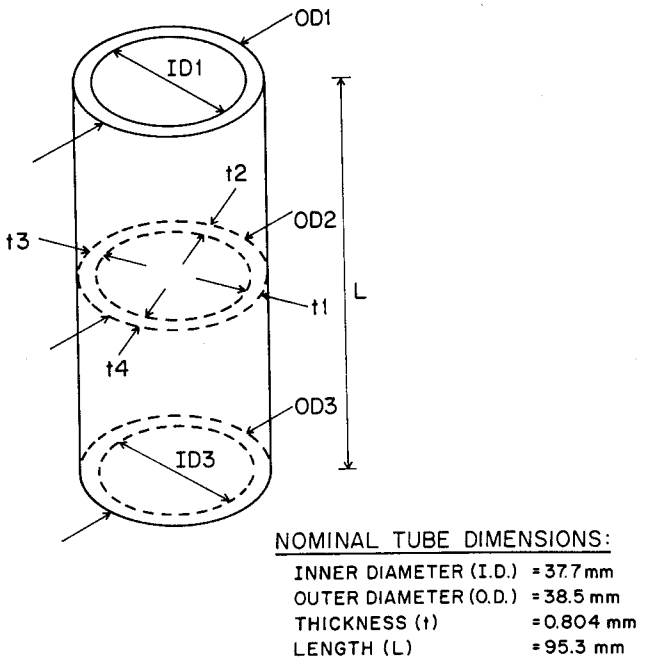

Fig. 3 Specimen dimensions and measurement locations for inner and outer diameters, thicknesses, and length.

was done in order to reduce the data to a standard independent of minor manufacturing variations. A typical specimen is illustrated in Fig. 3, along with the points at which measurements were taken.

The tubes were gaged with 0/90 rosette gages [120 Ω (EA-06-125TM-120) or 350 Ω (CEA-06-125UT-350)] and 120 Ω longitudinal gages (EA06-125AD-120), in order to measure longitudinal modulus. The measured longitudinal moduli were compared to predicted values as a means of quality control as reported in the next section.

All tubes were tested on an MTS 810 machine using special jigs designed for compression which provided two self-aligning flat surfaces. The test setup is pictured in Fig. 4. The top jig rotates around a ball bearing to align itself with the surface it contacts. Therefore, the jigs apply an even load on any specimen with two flat surfaces, whether or not the two surfaces are parallel. The tubes were loaded at a constant stroke rate of 0.762 mm/min, which is equivalent to a strain rate of approximately 8000 microstrain/min for a 95 mm long specimen. The maximum load was determined for each specimen and strain gage and load data were taken automatically with the use of a PDP-11/34 computer. Any noises indicative of damage were noted during the test and photographs were taken of the failed tube.

Results

The longitudinal moduli of the tubes were determined with the aid of a program developed at the Technology Laboratory for Advanced Composites, known as LIN6,[12] which determines linear regions of a data set. The stress was found by dividing the applied load by the nominal area (nominal thickness times π times nominal diameter). Moduli were determined for each longitudinal gage. The averages of these results for each layup type are reported in Table 2 along with the coefficients of variation. The predicted moduli as determined by classical laminated plate theory using the basic unidirectional ply are also reported. Good agreement is seen between the experimental and theoretical values of modulus with generally low coefficients of variation. This indicates that the specimens were acceptable for stress-strain data and did produce repeatable results.

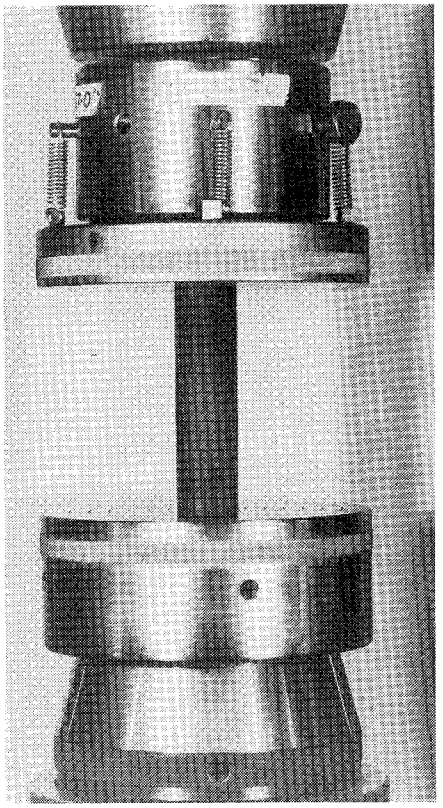

Fig. 4 Uniaxial compression test setup.

In determining the maximum load-carrying capacity of a specimen, care was taken so as not to halt the test prematurely due to slight decreases in the load. Local failures can and did cause decreases in the load, but further application of the stroke increased the load in some cases. The test was halted if either of the following two criteria were met: 1) brooming occurred at the specimen ends, since further loading would only result in further brooming and crushing of the tube ends; or 2) the load dropped by 25% of the maximum load attained to that point. Such a drop in load signals a permanent reduction in load-carrying ability.

The failure modes of the tubes can be grouped into five categories. The first two failure types involve in-plane fracture as the predominant mode. The first type is a fracture that is predominantly perpendicular to the applied load. The second type shows cracks that run in the matrix parallel to the fibers in the θ ply below the outer ply and thus fibers fracture along this same crack angle in the associated $-\theta$ and 0° plies. Two types of failure involve local instabilities as the predominant mode. The third type has shell buckling in part of or totally around the circumference of the tube. The fourth type, otherwise denoted as ply buckling, is observed when individual plies delaminate and buckle away from the remaining intact plies. The fifth type of failure is end damage such as the brooming previously described. Each of these modes is shown in Fig. 5.

The average failure stress and failure types are given in Table 3 for the $[\pm\theta/0]_s$ and $[0/\pm\theta]_s$ specimens. The failure types are numbered according to the key: 1) in-plane fracture, 2) in-plane splitting, 3) shell buckling, and 4) ply buckling. Of these 49, there were 14 tubes that failed as a result of end failure only. Since these results represent failures due to the testing procedure (i.e., end conditions), they are excluded from further consideration, as indicated in Table 3. In addition, of the two $[90_6]$ specimens, one had end failure, while the other failed at a stress of 208 MPa with a type 1 failure.

The failure of the $[0_6]$ specimens are delineated in Table 4 according to length-to-radius (L/R) ratios. It can be seen that there was no length-to-radius effect on the failure load and all

Table 2 Theoretical and experimental longitudinal moduli

	$[\theta_6]$			Experimental values				
				$[\pm\theta/0]_s$			$[0/\pm\theta]_s$	
θ,°	Calculated E_L, GPa	Measured E_L, GPa	CV, %	Calculated E_L, GPa	E_L, GPa	CV,%	E_L, GPa	CV,%
0	130	127	26.5	—	—	—	—	—
10	—	—	—	124	118	5.8	115	5.9
20	—	—	—	105	100	9.2	105	10.7
30	—	—	—	79.7	73.7	9.7	77.7	15.1
35	—	—	—	69.8	63.8	2.0	66.6	1.4
40	—	—	—	62.5	59.3	7.4	54.7	9.1
45	—	—	—	57.7	53.1	11.6	51.7	5.8
60	—	—	—	51.7	49.2	10.2	50.9	0.5
90	10.5	11.0	0.9	50.6	44.1	8.7	45.3	4.8

Table 3 Experimental failure stresses and modes for $[\pm\theta/0]_s$ and $[0/\pm\theta]_s$ specimens

	$[\pm\theta/0]_s$				$[0/\pm\theta]_s$			
θ,°	No. of tests excluded due to end failure	Failure stress, MPa	CV,%	Failure type(s)	No. of tests excluded due to end failure	Failure stress, MPa	CV,%	Failure types
10	1	356	16.8	3	0	324	4.8	1,3
20	1	409	21.6	1,2,3	0	363	7.2	3,4
30	1	285	18.9	2	0	310	20.5	1,2,3,4
35	1	370	—[a]	2	1	321	—[a]	2,4
40	1	343	—[a]	1,2	0	324	2.0	2,4
45	4	207	—[a]	2	1	276	22.4	1,4
60	1	165	—[a]	1	0	313	10.1	1,4
90	2	[b]	—[b]	[b]	0	251	16.2	1,4

[a]No CV reported since only one specimen failed not due to end failure. [b]No data reported since both specimens failed due to end failure.

Table 4 Experimental failure stresses for all $[0_6]$ specimens

L/R[a]	No. of specimens tested	Failure stress,[b] MPA	CV%
2	3	289	21.8
3	3	276	47.0
4	3	229	38.9
5	3	311	20.1
6	3	272	26.6
7	3	325	18.9
8	3	302	24.6
12	1	376	—
Total	22	290	26.0

[a]$R = 19.05$ mm (nominal). [b]All specimens failed in shell buckling (type 3).

of the tubes failed in shell buckling. This lack of dependence on L/R can be explained by the fact that shell buckling is independent of the length of the tube, except for effects of the geometric or natural boundary conditions near the ends of the tube. However, there was considerable scatter, which indicates that the irregularities in each of the tubes (both geometric and loading eccentricities) do affect the failure stress.

The failure stresses of the 57 specimens, excluding those with only end failure, are plotted vs the in-plane stress interaction criterion and equilibrium shell buckling predictions in Fig. 6 and 7 for the $[\pm\theta/0]_s$ and $[0/\pm\theta]_s$ laminate families, respectively. These predictions are represented by lines in each of the two figures. The predictions cross, thus implying that the failure mode of the specimen will change with the lamination angle. Note that the stress interaction criterion is based on the in-plane properties only and this prediction is thus independent of the stacking sequence. However, the shell buckling prediction is dependent on stacking sequence via the stacking sequence dependence of the bending terms that enter into the calculation.

The experimental failure stresses are generally much lower than the stresses predicted by either criterion. In some cases, this can be attributed to the fact that individual plies buckle and delaminate before in-plane fracture or shell buckling of the original laminate occurs. This reduces the load-carrying capability of the specimen, as is suggested in the next section.

Ply Buckling Model

The plies in a laminated composite can be modeled as individual orthotropic and homogeneous plates bonded at each ply interface. It has been shown that, at a ply interface, there is a thin region with only matrix material.[13] This interply matrix layer is on the order of one or two fiber diameters, as illustrated in Fig. 8. The laminate can thus be viewed as a series of plates connected by thin layers of epoxy. These layers of epoxy can further be modeled as springs that elastically connect individual plies, as illustrated in Fig. 9. This situation is similar to that of a plate on an elastic foundation. Out-of-plane stresses and displacements can result as individual plies buckle. In reality, eccentricities in loading exist from the onset of application; therefore, such out-of-plane deflections can occur immediately. The outermost plies are least restricted by the interconnecting springs and thus are most likely to buckle.

With this model in mind, a chain of events can be described that would lead to "premature" failure of the specimen at a stress below that predicted by other models (e.g., in-plane fracture or buckling of the entire laminate). During manufacture, voids and inclusions may be introduced in the ply interfaces. In addition, the thickness of the epoxy layer varies along the plane of the interface, thus changing the effective spring constant. The initial load is applied to the end surface, which may be skewed and not flat, thus causing eccentricities in the applied load. Out-of-plane deformations occur simultaneously with the application of load when an eccentricity or bending moment is present. As the outer plies undergo out-of-plane deformation, out-of-plane stresses arise. As a result of its deformed shape, the ability of the ply to carry load is decreased and the load is redistributed to the other plies. Further loading leads to further out-of-plane deflec-

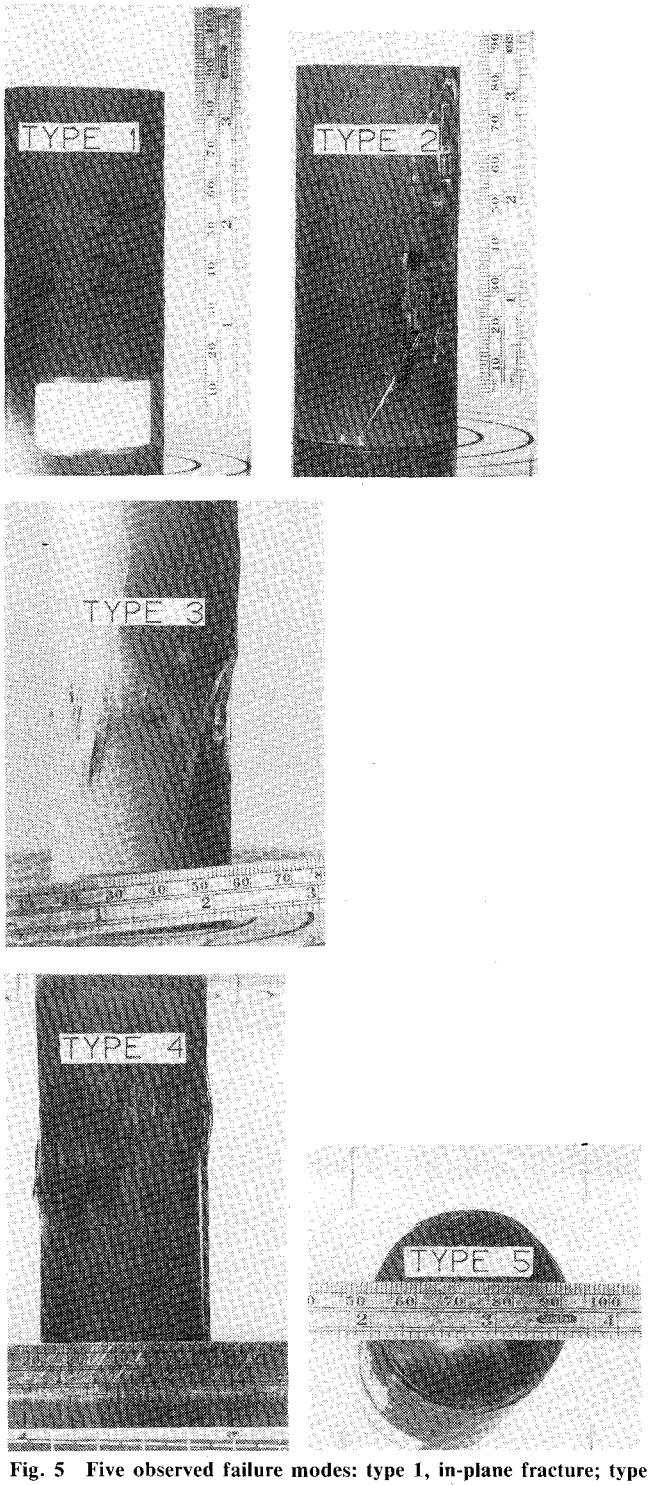

Fig. 5 Five observed failure modes: type 1, in-plane fracture; type 2, in-plane splitting; type 3, shell buckling; type 4, ply buckling; and type 5, end failure.

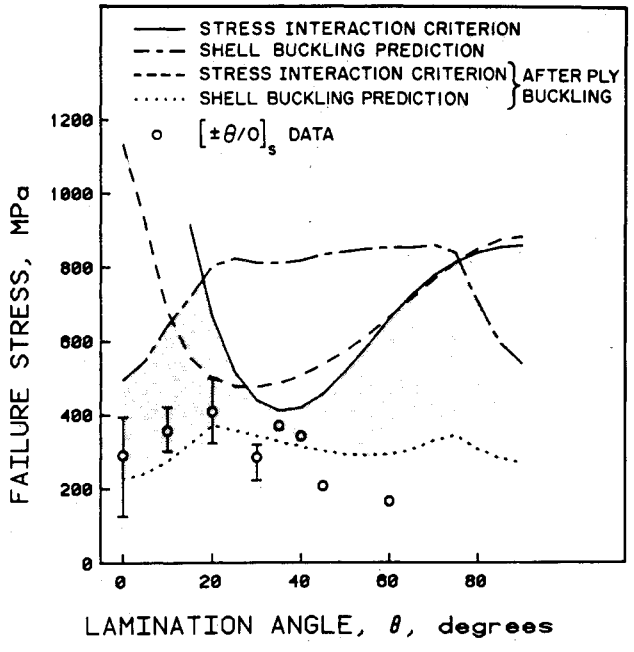

Fig. 6 Experimental failure stresses and theoretical correlations for $[\pm\theta/0]_s$ specimens.

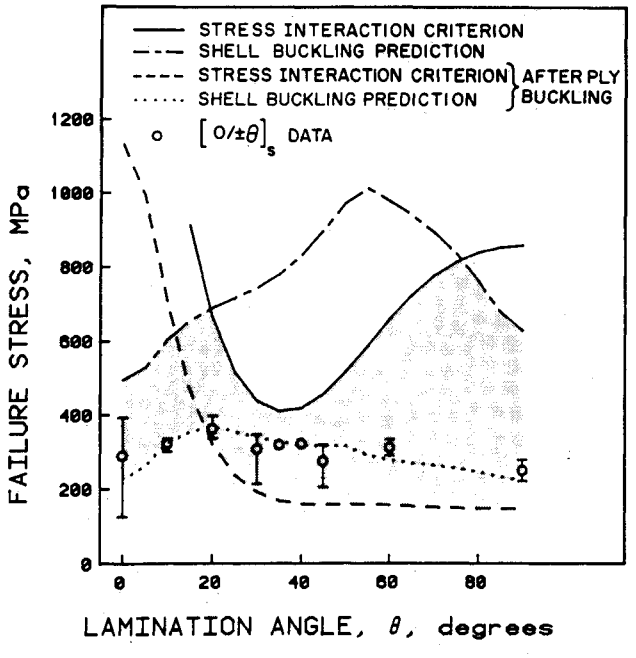

Fig. 7 Experimental failure stresses and theoretical correlations for $[0/\pm\theta]_s$ specimens.

tions. As the deflections increase, so do the normal and shear stresses in the epoxy layer. If the stresses become sufficiently high, the epoxy between the two plies will crack, creating a delamination. Voids or inclusions in this matrix interlayer are locations where delaminations are most likely to originate.

This sublaminate is now free to buckle without any restriction from the elastic foundation. A sublaminate is that portion of a laminate that is separated in the z direction (as defined in Fig. 1) from the remaining part of the laminate due to delamination. After the ply has buckled on the foundation, the ability of it to carry axial loads is reduced and the load is redistributed to the other plies. The out-of-plane deflections, and thus the radial stresses, can become so great as to cause massive delaminations.

Through this redistribution of load, other types of failure can be induced in the remaining intact plies. As the outer plies become ineffective, the bulk of the load is carried by the inner plies. This increment in stress can cause in-plane fracture or even induce buckling of the remaining intact piles.

In the extreme case, the load-carrying capability of the buckled plies is completely degraded, thus causing the load to be carried by the remainder of the laminate. Such an analysis can be performed by assuming that the moduli of the buckled plies are zero. A similar process where the load-carrying capability of the plies is degraded in order to determine final-ply failure in tension is discussed by Lagace.[14] Symmetric degradation is assumed.

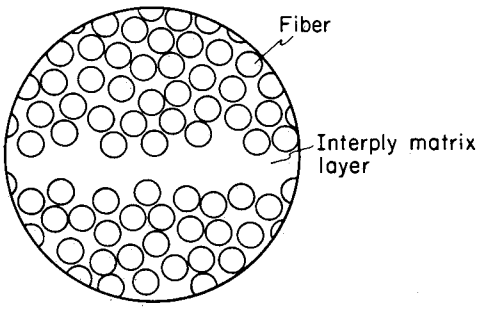

Fig. 8 Representative micrograph of an interply matrix layer.

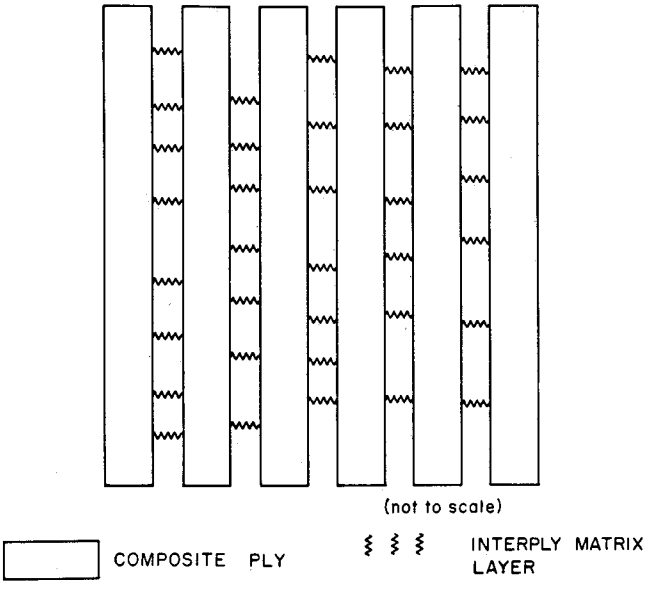

Fig. 9 Elastic foundation model of a six-ply laminate.

If the failure predictions (both in-plane fracture and shell buckling) are now performed on the laminate with the outer plies effectively removed, a lower bound to the region where failure might occur due to partial unloading of the outer plies can be found. Shown in Figs. 6 and 7 are the data plotted against the "feasible region" based on this ply buckling model. The feasible region at a given lamination angle has an upper bound determined by the lower of the fracture and shell buckling predictions for the intact laminate and has a lower bound determined by the lower of the fracture and shell buckling predictions based on the ply buckling model with the outermost ply, both inner and outer radius, "effectively" removed.

Since ply buckling is an out-of-plane phenomenon, it will depend on the stacking sequence. Moreover, the lamination angle of the outer plies will change with stacking sequence. This stacking sequence dependence is clearly shown in contrasting the predicted failure lines between the $[\pm\theta/0]_s$ laminates in Fig. 6 and the $[0/\pm\theta]_s$ layups in Fig. 7.

The concept of plies buckling independent of each other is not new. Both analytical and experimental studies[15-17] have been conducted in order to study the effect of an implanted delamination. In these studies, initial delaminations are created during manufacture by placing a piece of Teflon at a ply interface. Under compressive loading, the sublaminate debonds easily from the Teflon; buckles away from the remainder of the laminate; and causes the growth, stable or catastrophic, of the delamination. The major difference between these studies and the ply buckling model and work presented here is that this model relies on initial macroscopic imperfections and eccentricities to cause out-of-plane deformations and stresses.

Discussion

Expected failure types can be deduced from the boundaries of the feasible region and the intersections of the various failure criteria. For all values of lamination angle, the lower boundary of the feasible region for the $[\pm\theta/0]_s$ specimens is determined by shell buckling of the remaining intact plies after ply buckling. The upper boundary of the region for these specimens, however, is defined by shell buckling of the entire laminate for θ less than approximately 20° at which point the mode changes and the upper boundary is defined by in-plane fracture of the entire laminate. For values of lamination angle between 30° and 55°, the stress interaction criterion indicates that the loss of load-carrying capability due to ply buckling does not degrade (but actually slightly increases) the in-plane fracture strength of the laminate. For large values of θ (greater than 75°, shell buckling of the entire laminate again defines the upper boundary.

The experimental stresses for the $[\pm\theta/0]_s$ specimens generally lie within the feasible region, as can be seen in Fig. 6. Shell buckling was the failure mode for θ equal to 10° as predicted. For the $[\pm 20/0]_s$ specimens, a mixture of failure modes occurs: shell buckling and in-plane fracture (this includes both failure types 1 and 2). The upper bound of the feasible region suggests a transition of failure types should occur in this vicinity. For all larger values of lamination angle 30°, 35°, 40°, 45°, and 60°, the failure is due to in-plane fracture as suggested by the prediction. The data for the latter two angles, 45° and 60°, lie slightly below the feasible region. This might be attributed to irregularities in the tubes.

The feasible region for the $[0/\pm\theta]_s$ specimens, as defined in Fig. 7, is slightly more complex. In this case, the lower bound is determined by shell buckling after outer ply buckling only for θ less than 20°. For larger values of θ, in-plane fracture after the 0° plies have buckled away becomes the lower bound. As in the $[\pm\theta/0]$ case, shell buckling of the entire laminate defines the upper bound for small values of lamination angle (θ less than 20°) and for large values (θ greater than 75°). For all other values of θ, in-plane fracture of the entire laminate is the upper bound.

For the $[0/\pm\theta]_s$ specimens, the experimental failure stresses fall within the feasible region and very near the lower boundary. All specimens exhibited ply buckling except for the $[0/\pm 10]_s$ specimens, where a mixture of shell buckling and in-plane fracture occurred. For θ equal to 20°, shell buckling occurred after ply buckling as predicted. Several failure types occurred in the $[0/\pm 30]_s$ specimens. This is in the vicinity of the transition of failure types in the feasible region. For all larger values of the lamination angle (35°, 40°, 45°, 60°, and 90°) in-plane failure (either by fracture or splitting) follows ply buckling, as predicted using the ply buckling model. This was especially noticeable as θ increased with gross delaminations of the outer 0° plies occurring in the $[0/90_2]_s$ specimens prior to final failure.

It is important to note that, in the tubes which fractured parallel to the lamination angle, the matrix crack always occurred in the ply immediately below the outer ply. This observation is in line with the proposed phenomenon of ply buckling. If the outer ply buckles locally, the next ply is more susceptible to splitting as load is dumped to that ply from the buckled ply and the elastic constraint of the neighboring buckled ply is relaxed.

The phenomenon of ply buckling is not limited to a single ply, but may involve a group of plies buckling away from the remaining laminate. Two $[0_2/90]_s$ tubes, of the same configuration as previously described, were tested to examine this possibility. Both specimens failed as a result of ply buckling. However, the pair of 0° plies at the inner and outer radius delaminated away from the 90° plies. Final failure occurred as a result of fracture of the 90° plies at 386 MPa (the coefficient of variation is 3.9%). Thus, ply buckling seems to occur mainly between plies of different angles. This would explain the lack of influence ply buckling had on the failure of the $[0_6]$ tubes.

Summary

The tubes tested in this study failed at stresses that appear, at first hand, premature when compared to in-plane fracture and shell buckling predictions. Only after one introduces a ply buckling model do the failure stresses and failure types appear to be consistent. Such a phenomenon is inherent to laminated structures and must be accounted for in any design process. Degradation of a structure could occur at the onset of loading and such degradation could easily induce modes of failure at loads below the design load. Thus, designers must account for interactions among in-plane fracture, shell or plate buckling, and ply buckling in the design of laminated structures for compressive loading.

Acknowledgments

This work was supported by the Air Force Office of Scientific Research under Grant AFOSR-82-0071 and Contract F49620-83-K-0015. Dr. Anthony K. Amos was the contract monitor.

References

[1]Greszczuk, L.B., "Microbuckling Failure of Circular Fiber-Reinforced Composites," *AIAA Journal*, Vol. 13, Oct. 1975, pp. 1311-1318.

[2]deFerran, E.M. and Harris, B., "Compression Strength of Polyester Resin Reinforced with Steel Wires," *Journal of Composite Materials*, Vol. 4, Jan. 1970, pp.62-72.

[3]Lager, J.R. and June, R.R., "Compressive Strength of Boron-Epoxy Composites," *Journal of Composite Materials*, Vol. 3, 1969, pp. 43-56.

[4]Timoshenko, S.P., *Theory of Plates and Shells*, 2nd ed., McGraw-Hill Book Co., New York, 1959.

[5]Whitney, J.M., "Buckling of Anisotropic Laminated Cylindrical Plates," *Proceedings of the 24th Structures, Structural Dynamics and Materials Conference*, AIAA, New York, May 1983, pp. 563-568.

[6]Shuart, M.J., "An Evaluation of the Sandwich Beam Compression Test Method for Composites," *Test Methods and Design Allowables for Fibrous Materials*, ASTM STP 734, pp. 152-165.

[7]Hofer, K.E. Jr. and Rao, P.N., "A New Static Compression Fixture for Advanced Composite Materials," *Journal of Testing and Evaluation*, Vol. 5, No. 4, July, 1977, pp. 278-283.

[8]"Standard Test Method for Compressive Properties of Unidirectional or Crossply Fiber-Resin Composites," D 3410-75, *Space Simulation; Aerospace Materials; High Modulus Fibers and Composites, Annual Book of ASTM Standards*, Vol. 15.03, ASTM, Philadelphia, 1983, pp. 189-197.

[9]Tsai, S.W. and Wu, E.M., "A General Theory of Strength for Anisotropic Materials," *Journal of Composite Materials*, Vol. 5, Jan. 1971, pp. 58-80.

[10]Whitney, J.M. and Sun, C.T., "Buckling of Composite Cylindrical Characterization Specimens," *Journal of Composite Materials*, Vol. 9, April 1975, pp. 138-148.

[11]Tsai, S.W. and Hahn, H.T., *Introduction to Composite Materials*, Technomic Publishing Co., Westport, CT, 1980.

[12]Vizzini, A.J. and Lagace, P.A., "TELAC Software Manual," Technology Laboratory for Advanced Composites, Massachusetts Institute of Technology, Cambridge, in preparation.

[13]Wang, S.S., "Delamination Crack Growth in Unidirectional Fiber-Reinforced Composites under Static and Cyclic Loading," *Composite Materials: Testing and Design (Fifth Conference)*, ASTM STP 674, pp. 642-663.

[14]Lagace, P.A., "Static Tensile Fracture of Graphite/Epoxy," Ph.D. Thesis, Technology Laboratory for Advanced Composites Rept. 82-4, Massachusetts Institute of Technology, Cambridge, April 1982.

[15]Ashizawa, M., "Fast Interlaminar Fracture of a Compressively Loaded Composite Containing a Defect," Paper presented at Fifth DoD/NASA Conference on Fibrous Composites in Structural Design, New Orleans, Jan. 1981.

[16]Webster, J.D., "Flaw Criticality of Circular Disbond Defects in Compressive Laminates," Center for Composite Materials, University of Delaware, Newark, 1980-1981 Interim Rept., June 1981.

[17]Whitcomb, J.D., "Finite Element Analysis of Instability Related Delamination Growth," *Journal of Composite Materials*, Vol. 15, Sept. 1981, pp. 403-426.